Energy Equip. Sys. / Vol. 9/No. 4/Dec. 2021/ 383-395

ENERGY EQUIPSYS

Energy Equipment and Systems

http://energyequipsys.ut.ac.ir
www.energyequipsys.com

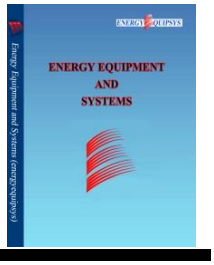

Investigation of the effect of Debye length change on electroosmotic flow with using constant density weakly compressible smoothed particle hydrodynamics method

Authors

Mojtaba Dehghanzadeh Bafghi[a]
Mohammad Sefid[a*]
Rahim Shamsoddini[b]
Amir Masoud Salehizadeh[a]

[a] Department of Mechanical Engineering, Yazd University, Yazd, Iran

[b] Department of Mechanical Engineering, Sirjan University of Technology, Sirjan, Iran

Article history:

Received : 6 April 2021
Accepted : 30 May 2021

ABSTRACT

Electroosmotic is one of the four electrokinetic phenomena that is formed by applying an electric field to an ionized electrolyte near the charged dielectric surface. Due to the applying of this electric field change the arrangement of ions within the electrolyte, and eventually a region called the Electric double layer is formed near the surface. The thickness of this layer is approximated by the Debye length. In this study, the Because the Reynolds number in in microfluidic devices is usually very low. Therefore, achieving to sufficient mixing in electroosmotic microchannel flow has been a challenge. For this purpose, a non uniform distribution of surface potential for flow mixing is considered. This type of charge distribution is very efficient for mixing purposes by creating circulations in the microchannel. Lagrangian description is used to solve the governing equations. The method used in this research is the constant density weakly compressible particle hydrodynamics method. In order to improve the mixing, the effect of changing the Debye length has been analyzed. The results show that increasing the Debye length causes smaller vortexes to be produced and mixing efficiency is reduced.

Keywords: Electroosmotic Flow, Debye Length, Rectangular Microchannels, Nonuniform Surface Potential.

1. Introduction

The electroosmotic phenomenon is crucial in the design and understanding of concepts such as reagents for laboratory chip systems and the analysis of biological systems. Because the reactions associated with these systems occur at the micron and even nanoscale, rapid mixing of samples is essential. Electroosmotic flow is critical in the design of Lab on a Chip systems and is widely used to transfer and mix liquids in micro and nanofluid systems. Pure electroosmotic flow in a microchannel is a smooth flow with no rotation and since it is a slow flow, there is no turbulence to stir the fluid. In microfluidic systems, it is very difficult and costly to use moving components to create turbulence. Therefore, mixing has always been a challenge in electroosmotic microscale systems. In general, microchannels are divided into active and inactive categories to increase mixing [1]. Passive micromixers usually use different geometric shapes to increase the contact surface of the mixed

* Corresponding author: Mohammad Sefid,
Department of Mechanical Engineering, Yazd University, Yazd, Iran.
Email: mhsefid@yazd.ac.ir

liquids and the main problem with passive mixing is the complexity of microscale fabrication. In active micromixers, an external driving force is used to create the mixture [2]. Recently, electroosmotic forces have been widely used in micromixers to control the movement of liquids. The characteristics of the electroosmotic flow in a microchannel depend on the nature of the potential of the channel surface, whether uniform or nonuniform.

Preliminary studies have been performed on electroosmotic flows with uniform surface electric potentials. Ajdari et al. [3] investigated the phenomenon of electroosmosis with nonuniform surface potential. They found that circulatinal zones by applying the surface potential opposite to the surface charge were created. Ren et al. [4] investigated the electroosmotic flow in circular microchannels by changing the axial pitch of the surface potential and observed perturbation velocity profiles in the flow. Erickson and Li [5] investigated the rotational regions in the flow in T-shaped micromixers with nonuniform surface potentials. They found that the rotation region is larger and stronger when the potential for a heterogeneous surface is equal to and opposite to a homogeneous surface. The velocity and potential distributions near the jump site in the surface potential have been analytically investigated by Yariv [6]. Fu et al. [7] obtained a stepwise change Based on the Nernst Planck equation for ion distribution in surface potential that causes a significant change in the velocity and pressure distribution. Lee et al. [8] analyzed the electroosmotic flow with nonuniform potential in a microchannel with assuming zero volumetric electric force outside the electric double layer. Tian et al. [9] observed that excellent mixing through nonuniform surface potential in microchannels may lead to very poor mass transfer. The effect of reservoirs at the beginning and end of a microchannel has been investigated by Mirbozorgi et al. [10]. Their results show that an inverse pressure gradient is created in the microchannel due to pressure drops due to the presence of reservoirs. Using different potentials in the horizontal electric field, different flow patterns can be created in the mixing chamber. The time dependent electroosmotic flow distributed by an alternating flow electric field with surface potential heterogeneity along the microchannel walls was investigated by Luo [11]. Bhattacharyya and Nayak [12] showed that the patch potential may increase the mixing of liquids in microchannels. Bhattacharyya and Nayak [13] found that surface geometry changes and surface potential heterogeneity cause more intense convection effects in nanochannels. Using experimental methods, Sun and Shie [14] experimentally investigated the performance of divergent intra microchannel mixing under electroosmotic flows with periodic potential and identified the optimal phase difference as well as the optimal half angle of divergence for the best mixing efficiency. Jain and Nandakumar [15] have used numerical optimization method to study different geometry formulations with different charge patterns and for each case have shown the optimal charge pattern for the maximum mixing rate. Sadeghi et al. [16] studied heat transfer in electroosmotic flows with excitation pressure and found that when the ratio of width to height of the channel increases, the Nusselt number generally increases. Cheng et al. [17] simulated electroosmotic mixing with periodic potentials using the Helmholtz Smolokowski model and concluded that vortexes induced by electroosmotic flows increase the quality of mixing at low frequencies while at the same frequency, high mixing is reduced.

In this research, the electrokinetic micropump have been investigated. Electrokinetichetic micropumps can be associated with pressure gradients, in which case they are referred to as electroosmootic / pressure driven micropumps, or they can be caused only by electrokinetic effects. Laplace, Poisson-Boltzmann and Momentum two-dimensional equations are solved numerically in a rectangular microchannel. Solving the nonlinear exponential term associated with the hyperbolic sine function in PoissonBoltzmann equation has always been a challenging task. In this study, it has been tried to solve this challenge by using the smooth particle hydrodynamics method and eliminating network dependencies. Because achieving higher mixing efficiency is one of the goals of micromixers, the effect of changing the Debye

length parameter on mixing has been investigated.

2. Geometry of case study

Figure 1 shows the proposed geometry for the Electroosmotic microchannel. This two dimensional microchannel has a height of *2H* and a length of *L*. It is exposed to the external electric field E_0 at both ends. The microchannel consists of a nonuniform charge distribution in the walls and its length is divided into 7 equal parts. Red lines show the negative charge $\psi_n=-|\zeta|$ with length $\frac{1}{7}L$, and blue lines show the positive charge $\psi_p=+|\zeta|$ with length $\frac{1}{7}L$.Also the patches, $\psi_0=0$ are without charge and have a length of $\frac{2}{7}L$ at the inlet and outlet of the channel so that the mid length of charged patches is $\frac{1}{7}L$.

The microchannel is filled with an electrolyte solution which is assumed to be a Newtonian fluid with constant properties. The parameters and constants used in this problem are given in Table 1.

3. Governing equations and boundary conditions

3.1. Poisson-Boltzmann equation

By placing the charged surface in the vicinity of the electrolyte solution, the surface reaction between the electrolyte ions and the adjacent surface causes the surface to become charged. The forces of attraction and repulsion between surface charges and the electrolyte change the arrangement of ions within the electrolyte, and eventually a region called the electric double layer is formed near the surface. In other words, the charged dielectric surface forms this region by absorbing ions opposite to its charge. As a result, there is a distribution of ions opposite the surface charge in the electric double region, while outside the electrolyte region is neutral. By applying an external

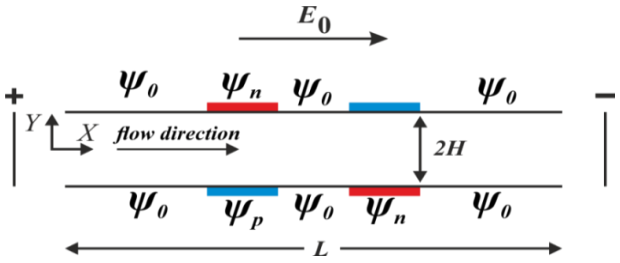

Fig. 1. The modelled two dimensional Electroosmotic microchannel

Table 1. Specifications of parameters and constants used in the modelled electroosmotic microchannel

Fluid density	ρ	$1000\left(\frac{kg}{m^3}\right)$
Permittivity of vacuum	ϵ_0	$8.854\times10^{-12}\left(\frac{F}{m}\right)$
Dielectric constant of the solution	ϵ_r	78.5
Valence	z	1
Electron charge	e	1.6×10^{-19} C
Boltzmann constant	k_b	$1.38\times10^{-23}\ \frac{J}{k}$
Absolute temperature	T	300K
External electric potential at the inlet	φ_{in}	10 v
External electric potentialat the outlet	φ_{out}	0 v
Microchannel Height	H	10 μm
Microchannel Length	L	140 μm
Diffusion coefficient	D	$10^{-12}\left(\frac{m^2}{s}\right)$

electric field on this electric double layer, a force is applied to the charges in this layer and this force causes the ions to move causing the fluid flow in the electric double layer. Finally, due to friction between the fluid layers, even the outer fluid flows from the electric double layer. This type of flow is called electroosmotic flow. Distribution of the electric potential in the solution due to dual electric layer ψ is described by Poisson-Boltzmann equation.

$$\nabla^2\psi = \frac{-\rho_f}{\dot{o}_0\dot{o}_r} \tag{1}$$

where the ψ potentials of the electric double region, ϵ_r and ϵ_0 represent the dielectric constants of the solution and Permittivity of vacuum, respectively. ρ_f is the free charge density is given:

$$\rho_f = ze\left(n_+ - n_-\right) \tag{2}$$

n_+ and n_- show the concentration of positive and negative ions, z represents the valance and e represents electron charge. The free charge density can be expressed in terms of the Boltzmann distribution, which for a symmetric solution $n_+=n_-=n$ using the Boltzmann distribution for ionic concentration:

$$\rho_f = -2ze\mathrm{n}_\infty \sinh\left(\frac{ze\psi}{k_bT}\right) \tag{3}$$

where n_∞ is bulk ionic number concentration, k_b is the Boltzmann constant, T is the absolute temperature. By placing Eq.(2) in Eq.(1) and using the Boltzmann distribution for the ionic species, the well-known Poisson Boltzmann equation is obtained as follows:

$$\frac{\partial^2\psi}{\partial x^2} + \frac{\partial^2\psi}{\partial y^2} = \frac{2zen_\infty}{\dot{o}_0\dot{o}_r}\sinh\left(-\frac{ze\psi}{k_BT}\right)) \tag{4}$$

The thickness of the electrical double layer is approximated by the debye length of λ_D. The Debye length is a characteristic of the electrolyte solution and depends on the molar concentration of the fluid, and its thickness can be estimated by the Debye–Huckel parameter λ_D^{-1}.

$$\lambda_D^{-1} = \frac{1}{\lambda_D} = \left[\frac{2z^2e^2n_\infty}{\dot{o}_0\dot{o}_rk_BT}\right]^{1/2} \tag{5}$$

To solve the Poisson-Boltzmann equation, the potential flux at the input and output is assumed to be zero.

$$\begin{cases} inlet\ x=0 & \partial\psi/\partial x = 0 \\ outlet\ x=L & \partial\psi/\partial x = 0 \end{cases} \tag{6}$$

And the pattern of zeta potential distribution on the microchannel wall is (as shown in Fig. 1):

$$\begin{cases} y=H & \psi=\zeta(x) \\ y=-H & \psi=-\zeta(x) \end{cases} \tag{7}$$

3.2. Laplace equation

In electroosmotic flows, the main idea is that by applying an external electric field such as φ to the electric charge of the electric double layer, the existing electrolyte can be moved. The application of this external electric field to a charged fluid results in the creation of a pure electric force $\rho_f E_0$, which is called the Lorentz force, in which E_0 is the external electric field strength $E_0 = \partial\varphi/\partial x$. The potential of an applied electric field φ is obtained by solving the Laplace equation.

$$\nabla^2\varphi = 0 \tag{8}$$

For an external electric field, a constant potential φ_{in} in is given at the inlet of the channel and a constant potential φ_{out} at the outlet of the channel is given, and the potential flux $\partial\varphi/\partial x$ is considered zero at the channel walls.

3.3. Continuity and momentum equations

When an electric current is applied the electric double layer, Electroosmotic flow is obtained. Two dimensional, incompressible, and laminar flow is intended for a Newtonian fluid. The governing equations are the mass conservation equation, the momentum equation, the state equation, and the concentration equation, respectively.

$$\frac{d\rho}{dt} = -\rho\nabla.V \tag{9}$$

$$\rho\frac{dV}{dt} = \mu\nabla^2V + \rho g - \nabla P + \rho_f E \tag{10}$$

$$P - P_0 = C^2\left(\rho - \rho_0\right) \tag{11}$$

$$\frac{dc}{dt} = D\nabla^2 c \tag{12}$$

In Eqs.(9-12), ρ is the density, V is the velocity, P is the pressure, g is the gravitational acceleration, μ is the viscosity of the fluid, D is the mass diffusion coefficient, c is the concentration and C is the sound velocity, and d represents the material derivative. $\rho_f E$ is the volumetric force caused by the application of an electric field acting on a fluid equal to:

$$E = -\nabla\Phi \tag{13}$$

where Φ is the total potential due to the linear sum of the potential of the electric double layer ψ and the potential of the applied electric field φ (i.e. $\Phi = \psi + \varphi$). At the channel inlet, to eliminate the frictional and shape change effects, a parabolic velocity distribution with a maximum velocity u_{in} is used, which represents a fully developed flow rate. To solve the momentum equation, the vertical and horizontal velocities in the channel walls are assumed to be zero. A fully developed condition is used for the velocity at the channel outlet.

$$\begin{cases} inlet\ x = 0 & \dfrac{u}{u_{in}} = \left[1 - \left(\dfrac{y}{H}\right)^2\right] \quad , v = 0 \\ outlet\ x = L & \partial u / \partial x = 0 \quad , \partial v / \partial x = 0 \end{cases} \tag{14}$$

There is no slip in the channel walls and the nonslip boundary condition is used ($u = v = 0$ in $y = \pm H$).

In order to evaluate the mixing quality, the mixing efficiency is defined, which shows the mixing performance at each cross section of the microchannel and is defined as follows.

$$\sigma(x) = \left(1 - \frac{\int_{-H}^{+H} |c - c_\infty| dy}{\int_{-H}^{+H} |c_0 - c_\infty| dy}\right) \tag{15}$$

where c_0 and c_∞ are the concentrations of the species not fully mixed and completely mixed, respectively.

4. Smooth particle hydrodynamics method

4.1. Formulation

The smooth particle hydrodynamics (SPH) approach is used to solve the governing equations of the flow. SPH is a mesh free Lagrangian discretization scheme in which the continuous environment is discretized with a limited number of computational points. SPH uses an integral representation method in a weak form using a smoothing function with an interpolation domain called the support domain. If f is an arbitrary function in the support domain Ω we can write:

$$f(r) = \int_\Omega f(r') W(r - r', h)\, dr' \tag{16}$$

where r and r' are the position vectors and the sub integral variable, W is called the smoothing or kernel function, and h is called the smooth length. Equation (16) can be approximated as a series of discretization in the domain Ω.

$$f(r) = \sum_{j=1} \omega_j f_j W(r - r', h) \tag{17}$$

In this study, the fifth-order Wendland kernel is used for the kernel function [18]. This recent research has shown that using this function causes to the required computational accuracy and cost for most cases.

$$W(r,h) = 7/\pi h^2 \begin{cases} (1-s)^4 (4s+1) & 0 \le s \le 1 \\ 0 & s \ge 1 \end{cases} \tag{18}$$

The first derivative of an arbitrary function f in the particle i can be approximated using the following general form.

$$\nabla f_i = \sum_j G_{ij} (f_j - f_i) \tag{19}$$

where j represents the neighboring particles of the particle i. f_j is the value of f in particle j, and G_{ij} is a weight function that shows the contribution of particle j to particle i. The values of G_{ij} are a function of the relative position vector of the neighbors of particle i, ie $r_{ij} = r_j - r_i$.

$$G_{ij} = \omega_j B_i . \nabla W_{ij} \tag{20}$$

Here ω_j is an infinitesimally small volume for a particle j and is defined as $\omega_j = m_j/\rho_j$, which in this study has a constant value for all SPH particles. Also, $W_{ij} = W(r_{ij}, h)$ is athe smoothing or kernel function which is a smoothed version of the Dirac Delta function and is a positive value for $r_{ij} = |r_{ij}| < h$ [19]. Tensor B is also the first order normalizing tensor previously introduced by Bonet and Lok [20] to correct the first order derivative of the kernel function.

$$B_i = -\left[\sum_j \omega_j \nabla W_{ij} \otimes r_{ij}\right]^{-1} \quad (21)$$

The second order derivative uses the same pattern as the first derivative but with different weights [21].

$$\nabla.\nabla f_i = \sum_j Q_{ij}\left(f_j - f_i\right) \quad (22)$$

As described in [21], a second-order Laplacian consistent scheme can be expressed as:

$$Q_{ij} = 2\hat{B}_i : \lambda_{ij} \quad (23)$$

where,

$$\lambda_{ij} = \omega_j \left(\frac{e_{ij}}{r_{ij}} \otimes \nabla W_{ij} + S_{e2}.B_i.\nabla W_{ij}\right) \quad (24)$$

where $e_{ij} = r_{ij} / \left|r_{ij}\right|$ and $S_{e2} = \sum_j \omega_j e_{ij} e_{ij} \nabla W_{ij}$. Also $\hat{B}_i$ is the normalized Laplacian tensor given by the following equation:

$$\hat{B}_i : Z_i = I \quad (25)$$

where in:

$$Z_i = \sum_j \lambda_{ij} \mathrm{r}_{ij} \mathrm{r}_{ij} \quad (26)$$

4.2. Constant density weakly compressible particle hydrodynamics for electroosmotic flows

First, the external potential field φ is solved.

$$\nabla^2 \varphi = 0 \quad (27)$$

To solve the Poisson Boltzmann equation, the Taylor expansion of the *sinh* function has been used. The main challenge in all numerical studies is the exponential nonlinearity of this term. Using the Taylor expansion, Eq.(4), Poisson-Boltzmann equation, is modified and discretized as follows.

$$\sum_j 2\omega_j \left(\psi_i^{k+1} - \psi_j^{k+1}\right) \frac{e_{ij}.\left(B_i.\nabla W_{ij}\right)}{\left|r_{ij}\right|} = \frac{2zen_\infty}{\dot{o}}\left[sinh\left(\frac{ze\psi_i^k}{k_B T}\right) + \frac{ze}{k_B T}\left(\psi_i^{k+1} - \psi_i^k\right) cosh\left(\frac{ze}{k_B T}\psi_i^k\right)\right] \quad (28)$$

The uppercase *k* shows the value calculated in the previous iteration and the uppercase *k + 1* shows the value in the new iteration. Inserting the Eq.(11) in Eq.(9) and rearrangements it is deduced that:

$$\frac{1}{c^2}\frac{dp}{dt} = -\rho \nabla.V \quad (29)$$

Here, a modified form of the algorithm is applied. The procedure is that first, the middle mean velocity field ($\tilde{V}$) is estimated without using the pressure term.

$$\rho\left(\frac{\tilde{V} - V^n}{\Delta t}\right) = \mu \nabla^2 V^n + \rho g + \frac{\rho_f E}{\rho} \quad (30)$$

Combining Eq.(30) and Eq.(29), the following equation can be deduced:

$$V^{n+1} = \tilde{V} - \frac{\nabla P^n}{\rho} \quad (31)$$

Then, by applying divergence to Eq. (31) and placing it in Eq.(29), then the new pressure is calculated by the following equation.

$$\frac{P^{n+1} - P^n}{\Delta t} = -\rho c^2 \left(\Delta.\tilde{V} - \Delta t \frac{\nabla.\nabla P^n}{\rho}\right) \quad (32)$$

In the next step, the new speed is calculated using the following equation.

$$V^{n+1} = \tilde{V} - \Delta t \frac{\nabla P^{n+1}}{\rho} \quad (33)$$

Equations (30) to (33) form a predictive corrective scheme similar to the methods explained in references [22] and [23] with some corrections and mathematical manipulations. The main difference here is that the density is assumed to be constant. This algorithm greatly alters the extreme fluctuations of the standard method of wickly compressible smooth particle hydrodynamics. Finally, the new position of the particles is calculated as follows:

$$r^{n+1} = r^n + V^{n+1}\Delta t \quad (34)$$

If the mass transfer equation needs to be solved, Eq.(12) is solved as follows.

$$c^{n+1} = c^n + \alpha \nabla^2 c^n \Delta t \quad (35)$$

According to the idea of Shadloo et al. [24] at the end of each time step, all internal particles are displaced according to the following equation.

$$\Delta r_i = \dot{o} V_i \Delta t \sum_j \left(\frac{d_0}{r_{ij}}\right)^3 e_{ij} \quad (36)$$

where d_0 is the distance of the initial particles (from the reference point based on the Lagrangian description) and ϵ can take a value between 0 and 0.1.

After placing the particle in the new position, it is necessary to correct the values of other field variables as well. Hence, the expansion of the first sentence of the Taylor series is used as follows for other variables.

$$\Delta\varphi_i = \Delta r_i.\nabla\varphi_i \tag{37}$$

$$\Delta\psi_i = \Delta r_i.\nabla\psi_i \tag{38}$$

$$\Delta V_i = \Delta r_i.\nabla V_i \tag{39}$$

$$\Delta P_i = \Delta r_i.\nabla P_i \tag{40}$$

$$\Delta C_i = \Delta r_i.\nabla C_i \tag{41}$$

Virtual particles are used to apply boundary conditions. These particles have been used according to the design of Lee et al. [25]. These particles have a velocity equal to the velocity of the corresponding wall particles and also for the stationary wall, in the direction perpendicular to the wall, they have the same pressure equal to that of the wall particle. A numerical code has been implemented to solve electroosmotic flows based on the constant density weakly compressible particle hydrodynamics method. The solution algorithm is expressed in Pseudo code in Table 2.

5. Validation of results and independence of solution from the particle

Accuracy of the program has been validated with a model that has already been solved analytically and numerically by Dutta and Beskok [26]. This model includes a two dimensional microchannel with a height of 2H and a length of $L_1 + L_2 + L_3$. The length of the channel is divided into three parts. According to Fig. 2, the middle part contains a material that has some electroosmotic effects, while these effects are neglected for the beginning and end of the channel. The channel is filled with a Newtonian electrolyte fluid of constant density and viscosity. The height of the channel is $H = 10\mu m$ and the length of each part of the channel is $L_1, L_2, L_3 = 31\ \mu m$. The geometry of this numerically modelled problem is shown in Fig. 2.

Table 2. Summarizes the computational algorithm

for each time-step n do
find the neighboring particles;
for each particle i do
compute φ using Eq. (27) ;
compute ψ using Eq. (28) ;
compute $\tilde{V}$ using Eq. (30);
end for
for each internal particle i do
compute P^{n+1} using Eq. (32);
end for
update pressure of wall particles;
for each internal particle i do
compute V^{n+1} using Eq. (33);
end for
for each internal particle i do
compute r^{n+1} using Eq. (34);
end for
if mass transfer is active then
calculate c^{n+1} using Eq. (35);
end if
for each internal particle i do
shift the position by Δr_i evaluated from Eq. (36);
correct the electric double layer potentials, external potential, velocity, pressure, concentration using Eqs. (37) to (41);
end for
end for

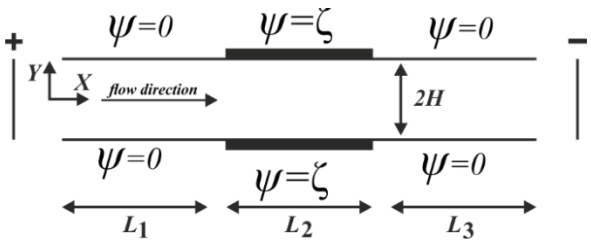

Fig. 2. Modeling of a two dimensional electroosmotic microchannel adopted from reference [26]

Velocity components in x and y directions are normalized with reference velocity U_{ref} (i.e. $U = u/U_{ref}$ and $V^* = v/U_{ref}$) and the coordinates in the longitudinal and transverse directions are normalized with respect to half height of the channel H (i.e. ($\xi = x/H$ and $\eta = y/H$). The reference velocity U_{ref} is calculated based on the Reynolds reference $Re_{ref} = 0.005$. Fig. 3 shows the axial dimensionless velocity in terms of dimensionless width at the center of the channel, i.e. $\xi = 4.5$ for $U_{in} = 2$. The compatibility of the solution results with the reference solution [26] is evident.

Also, to investigate the convergence and solubility independence of the particle, the velocity distributions for three different particle distances $\Delta x = 4 \times 10^{-7}$, $\Delta x = 2.5 \times 10^{-7}$ and $\Delta x = 2 \times 10^{-7}$ have been examined. Considering these three particle distances, Fig. 4 shows the numerical solution values of the dimensionless velocity distribution in the middle of the channel with $U_{in} = 2$. These results show the velocity convergence at $\Delta x = 2 \times 10^{-7}$ as compared to those results given in the reference solution [26].

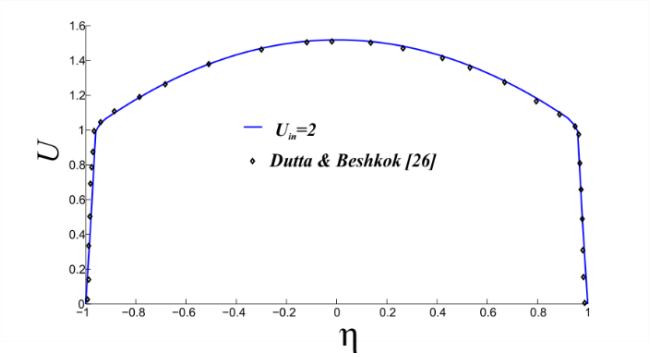

Fig. 3. Dimensional velocity distribution in the center of the channel for different $\boldsymbol{U_{in}}$. These numerical results are compared with those given in the reference [26].

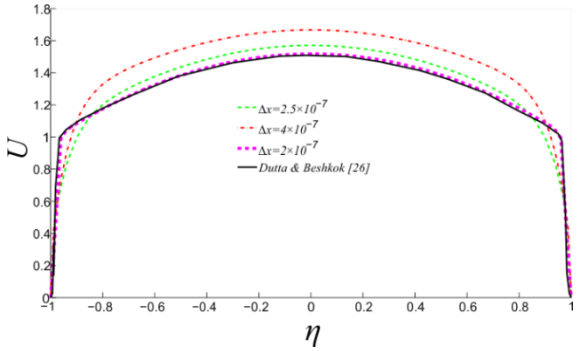

Fig. 4. Dimensional velocity distribution in the center of the channel for $\boldsymbol{U_{in} = 2}$ for the three particle spacing $\boldsymbol{\Delta x = 4 \times 10^{-7}}$, $\boldsymbol{\Delta x = 2.5 \times 10^{-7}}$ and $\boldsymbol{\Delta x = 2 \times 10^{-7}}$ and comparison with reference solution [26].

6. Results and Discussion

The geometry shown in Fig. 1 is solved numerically. For a dimensionless solution, as in the steps in validating the results, the parameters are dimensionless and Reynolds's base is $Re_{ref} = 0.005$. The thickness of the electric double layer also affects the flow. As mentioned earlier, the approximate thickness of the electric double layer is determined by the Debye length. A strong electrolyte solution has a higher molar concentration compared to that of a weak electrolyte solution with a thinner Debye length. To investigate the effect of the thickness of the electric double layer on the flow, a comparison was made between the two Debye lengths $\lambda_D = 2\mu m$ and $\lambda_D = 0.78\mu m$ for the zeta potential $\zeta = -11\, mv$. The maximum velocity at the center of the microchannel is assumed to be $u_{in} = 0.15\, mm/s$. Fig. 5 shows a dimensionless horizontal velocity contour with streamlines for the two Debye lengths $\lambda_D = 2\mu m$ و $\lambda_D = 0.78\mu m$ and a zeta potential ζ = -11 *mv*. As shown in the figure, the shorter Debye length results in higher velocity values. Two symmetric vortexes are created due to the asymmetric effects of the potential cgarge on the surface. Vortexes with shorter Debye lengths have achieved positive and negative velocities with higher values. These phenomena, result in greater mixing of flow swith stronger electrolytes or give thinner thicknesses of the electric double layer.

Figure 6 shows the potential distribution of an electric double layer at position ξ=5 for the two Debye lengths in question. As it is observed from the figure, the slope of the potential change for $\lambda_D = 0.78\mu m$ is steeper than that of obtained for $\lambda_D = 2\mu m$. This phenomenon results in a stronger electroosmotic force during the lower Debye because the electroosmotic force is directly related to the potential gradient. In the position of ξ=5, the upper patch has a negative charge (shown in red in Fig. 6) and the lower patch has a positive charge (shown in blue in Fig. 6). In the middle of the microchannel, the potential distribution is zero, indicating that there is no electroosmotic force in the middle of the channel.

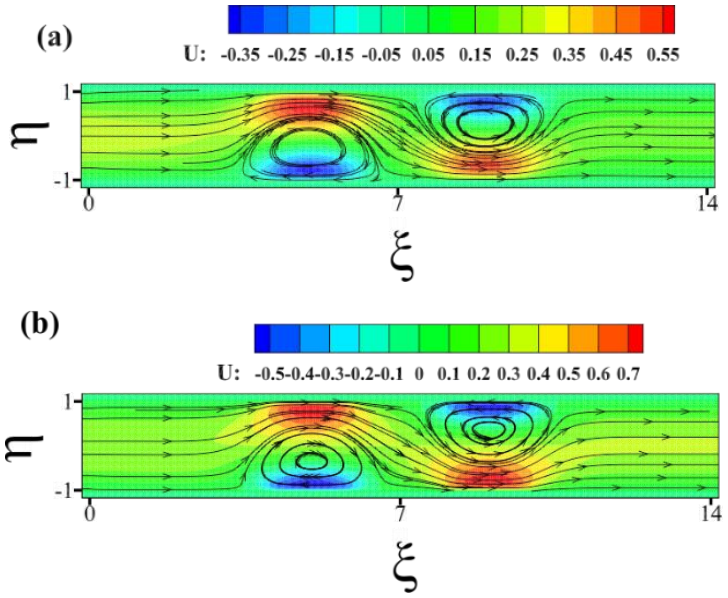

Fig. 5. Dimensional horizontal velocity contours with stremlines for potential *ζ=-11 mv.* a) $\boldsymbol{\lambda_D = 2\mu m}$ b) $\boldsymbol{\lambda_D = 0.78\mu m}$

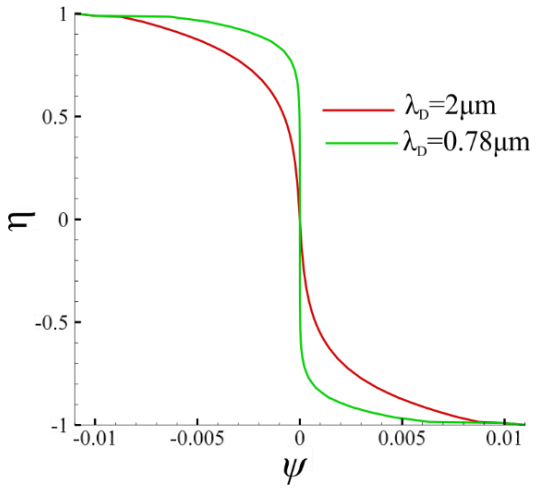

Fig. 6. Potential distribution of the electric double layer at ξ=5 for $\boldsymbol{\lambda_D = 2\mu m}$ and $\boldsymbol{\lambda_D = 0.78\mu m}$

Fig. 7 shows the dimensionless velocity contour in the vertical direction for the two Debye lengths $\lambda_D = 2\mu m$ and $\lambda_D = 0.78\mu m$. At the beginning of the channel, due to fully developed vertical flow, the vertical velocity is zero, but the flow is affected by electroosmotic forces when entering the first asymmetric patch of the charge and appears in the vertical direction to change the velocity profile and create a vortex. At the beginning of the microchannel, the velocity is in the vertical direction. When fluid enters the first patch, the velocity values are positive and upwards, and at the exit of the channel, the vertical velocity values are negative and downward. Then, at the entrance to the second patch, the opposite patch acts and causes a vortex in clockwise direction. The velocity values in the upper figure are plotted for $\lambda_D = 2\mu m$. They are lower than those shown in the lower figure for $\lambda_D = 0.78\mu m$, indicating that the electroosmotic forces are more intense during the lower Debye, or in other words the thickness of the electrical double layer is thinner so that larger velocities are created and result in more intense mixing.

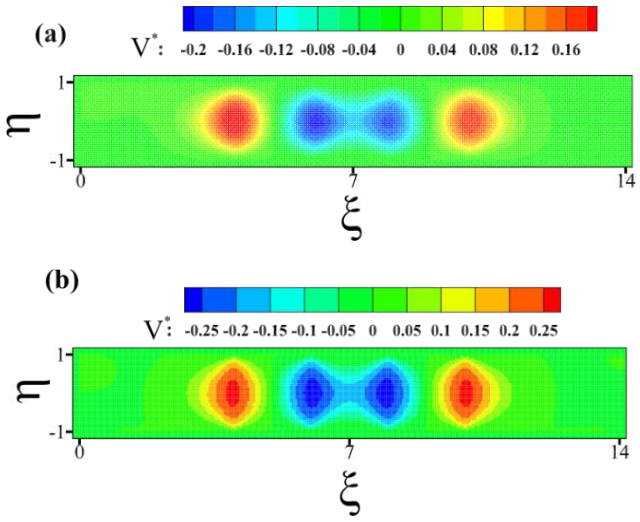

Fig. 7. Dimensional vertical velocity contours with flow lines for zeta potential *ζ=-11 mv.* a) $\boldsymbol{\lambda_D = 2\mu m}$ b) $\boldsymbol{\lambda_D = 0.78\mu m}$

Figure 8 shows a dimensionless vertical velocity profile in the longitudinal section at the center of the microchannel ($\eta = 0$) for the two Debye lengths in question. As shown in the figure, the maximum and minimum points related to the Debye length $\lambda_D = 0.78\mu m$ are superior to those of $\lambda_D = 2\mu m$, which indicates that the electroosmotic forces act less strongly for lower Debye length and the values of larger vertical velocities are greater than those achieved for greater Debye length. Due to the symmetry in the geometry and charge distribution, the symmetry in the vertical velocity profiles is also evident.

Figure 9 shows the mixing efficiency for the two Debye lengths $\lambda_D = 2\mu m$ and $\lambda_D = 0.78\mu m$. As it is evident from the figure, the flow in the microchannel mixes more with a smaller Debye length and the mixing efficiency increases by about 38% at the channel outlet. It may be concluded that the mixing increases with decreasing in Debye length or in other words the thickness of the double electric layer is reduced for this condition.

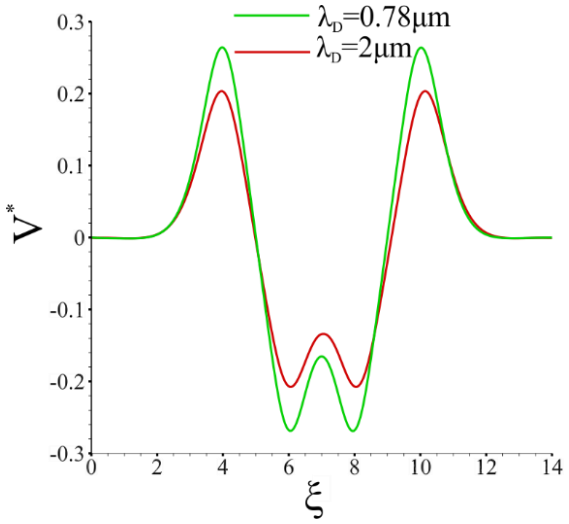

Fig. 8. Dimensionless vertical velocity profile in the middle longitudinal section of the microchannel with potential *ζ=-11 mv.* for $\boldsymbol{\lambda_D = 2\mu m}$ and $\boldsymbol{\lambda_D = 0.78\mu m}$

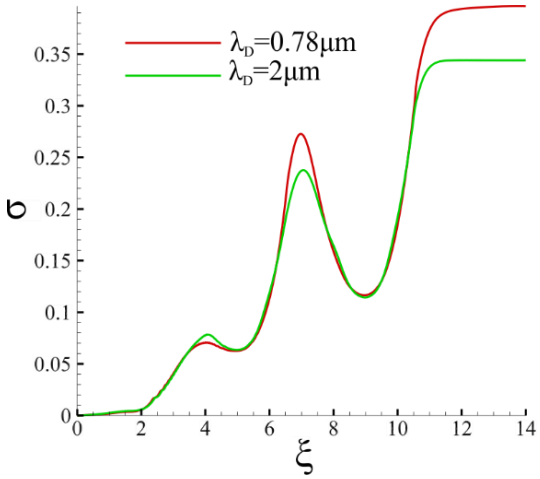

Fig. 14. The mixing efficiency with zeta potential *ζ=-11 mv* for the two Debye lengths $\boldsymbol{\lambda_D = 2\mu m}$ and $\boldsymbol{\lambda_D = 0.78\mu m}$

7. Conclusion

Two dimensional microchannels with asymmetric charge distribution under the simultaneous effects of pressure gradient and electroosmotic force have been studied. Flow characteristics are obtained by solving the Poisson Boltzmann and Navier-Stokes equations based on Lagrangian description and using the constant density weakly compressible particle hydrodynamics method. Distributing the potential charge with opposite signals on the surface creates a reverse electroosmotic force, resulting in circulational zones in the flow. The results show that increasing the Debye length or in other words increasing the thickness of the electric double layer produces weaker horizontal and vertical velocity fields which also reduces the effect of mixing. It is also concluded that with increasing the length of the Debye, the gradient decreases the ψ potential so that weak electroosmotic forces are obtained.

Acknowledgements: Nothing has been said by the authors.

Conflict of interest: There is no conflict of interest.

References

[1] Capretto L, Cheng W, Hill M, Zhang X. Micromixing within microfluidic devices. Microfluidics: Springer; 2011. p. 27-68.

[2] Liu S, Dasgupta PK. Electroosmotically pumped capillary flow-injection analysis: valve-based injection systems and sample throughput. Analytica chimica acta. 1993;283(2):739-45.

[3] Ajdari A. Electro-osmosis on inhomogeneously charged surfaces. Physical Review Letters. 1995;75(4):755.

[4] Ren L, Li D. Electroosmotic flow in heterogeneous microchannels. Journal of colloid and interface science. 2001;243(1):255-61.

[5] Erickson D, Li D. Influence of surface heterogeneity on electrokinetically driven microfluidic mixing. Langmuir. 2002;18(5):1883-92.

[6] Yariv E. Electro-osmotic flow near a surface charge discontinuity. Journal of Fluid Mechanics. 2004;521:181.

[7] Fu L-M, Lin J-Y, Yang R-J. Analysis of electroosmotic flow with step change in zeta potential. Journal of Colloid and Interface Science. 2003;258(2):266-75.

[8] Lee JS, Ren CL, Li D. Effects of surface heterogeneity on flow circulation in electroosmotic flow in microchannels. Analytica Chimica Acta. 2005;530(2):273-82.

[9] Tian F, Li B, Kwok DY. Tradeoff between mixing and transport for electroosmotic flow in heterogeneous microchannels with nonuniform surface potentials. Langmuir. 2005;21(3):1126-31.

[10] Mirbozorgi S, Niazmand H, Renksizbulut M. Electro-osmotic flow in reservoir-connected flat microchannels with non-uniform zeta potential. 2006.

[11] Luo W-J, Yarn K-F, Hsu S-P. Analysis of electrokinetic mixing using AC electric field and patchwise surface heterogeneities. Japanese journal of applied physics. 2007;46(4R):1608.

[12] Bhattacharyya S, Nayak A. Electroosmotic flow in micro/nanochannels with surface potential heterogeneity: An analysis through the Nernst–Planck model with convection effect. Colloids and Surfaces A: Physicochemical and Engineering Aspects. 2009;339(1-3):167-77.

[13] Bhattacharyya S, Nayak A. Combined effect of surface roughness and heterogeneity of wall potential on electroosmosis in microfluidic/nanofuidic channels. Journal of Fluids Engineering. 2010;132(4).

[14] Sun C-l, Shie S-S. Optimization of a diverging micromixer driven by periodic electroosmotics. Microsystem technologies. 2012;18(9-10):1237-45.

[15] Jain M, Nandakumar K. Optimal patterning of heterogeneous surface charge for improved electrokinetic micromixing. Computers & Chemical Engineering. 2013;49:18-24.

[16] Sadeghi A, Azari M, Chakraborty S. H2 forced convection in rectangular microchannels under a mixed electroosmotic and pressure-driven flow. International Journal of Thermal Sciences. 2017;122:162-71.

[17] Cheng Y, Jiang Y, Wang W. Numerical simulation for electro-osmotic mixing under three types of periodic potentials in a T-shaped micro-mixer. Chemical Engineering and Processing-Process Intensification. 2018;127:93-102.

[18] Wendland H. Piecewise polynomial, positive definite and compactly supported radial functions of minimal degree. Advances in computational Mathematics. 1995;4(1):389-96.

[19] Gingold RA, Monaghan JJ. Smoothed particle hydrodynamics: theory and application to non-spherical stars. Monthly notices of the royal astronomical society. 1977;181(3):375-89.

[20] Bonet J, Lok T-S. Variational and momentum preservation aspects of smooth particle hydrodynamic formulations. Computer Methods in applied mechanics and engineering. 1999;180(1-2):97-115.

[21] Fatehi R, Manzari M. A remedy for numerical oscillations in weakly compressible smoothed particle hydrodynamics. International Journal for Numerical Methods in Fluids. 2011;67(9):1100-14.

[22] Sefid M, Fatehi R, Shamsoddini R. A modified smoothed particle hydrodynamics scheme to model the stationary and moving boundary problems for Newtonian fluid flows. Journal of Fluids Engineering. 2015;137(3).

[23] Shamsoddini R, Sefid M, Fatehi R. Lagrangian simulation and analysis of the micromixing phenomena in a cylindrical paddle mixer using a modified weakly compressible smoothed particle hydrodynamics method. Asia-Pacific Journal of Chemical Engineering. 2015;10(1):112-24.

[24] Shadloo MS, Zainali A, Sadek SH, Yildiz M. Improved incompressible smoothed particle hydrodynamics method for simulating flow around bluff bodies. Computer methods in applied mechanics and engineering. 2011;200(9-12):1008-20.

[25] Lee E-S, Moulinec C, Xu R, Violeau D, Laurence D, Stansby P. Comparisons of weakly compressible and truly incompressible algorithms for the SPH mesh free particle method. Journal of computational Physics. 2008;227(18):8417-36.

[26] Dutta P, Beskok A, Warburton TC. Numerical simulation of mixed electroosmotic/pressure driven microflows. Numerical Heat Transfer: Part A: Applications. 2002;41(2):131-48.